Supplementary information

Is Cu instability during the CO_2 reduction reaction governed by the applied potential or the local CO concentration?

Patrick Wilde, [a,Δ] Peter B. O'Mara, [b,Δ] João R. C. Junqueira,[a] Tsvetan Tarnev,[a] Tania M. Benedetti,[b] Corina Andronescu,[c] Yen-Ting Chen,[d] Richard D. Tilley,[*,b,e] Wolfgang Schuhmann,[*,a] J. Justin Gooding,[*,b,f]

[a.] *Analytical Chemistry - Center for Electrochemical Sciences (CES), Faculty of Chemistry and Biochemistry, Ruhr-Universität Bochum, Universitätsstr. 150, D-44780 Bochum, Germany. E-mail: wolfgang.schuhmann@rub.de*
[b.] *School of Chemistry and Australian Centre for NanoMedicine, University of New South Wales, Sydney 2052, Australia. E-mail: justin.gooding@unsw.edu.au; r.tilley@unsw.edu.au*
[c.] *Chemical Technology III, Faculty of Chemistry and CENIDE, Center for Nanointegration University Duisburg Essen, Carl-Benz-Str. 199; D-47057 Duisburg, Germany*
[d.] *Center for Solvation Science (ZEMOS), Ruhr-Universität Bochum, Universitätsstr. 150, D-44780 Bochum, Germany*
[e.] *Electron Microscope Unit, Mark Wainwright Analytical Centre, University of New South Wales, Sydney 2052, Australia*
[f.] *Australian Research Council Centre of Excellence in Convergent Bio-Nano Science and Technology, University of New South Wales, Sydney 2052, Australia*
Δ. These authors contributed equally.

Table of Contents

Page S2-S3 Materials, Methods

Page S4 ELC-TEM

Page S5 Figure S1, S2

Page S6 Figure S3

Page S7 Figure S4, S5

Page S8 Figure S6, S7

Page S9 Figure S8, S9

Page S10 Figure S10, S11

Page S11 Figure S12, References

Materials

All chemicals were obtained from commercial suppliers and used without further purification. Silver (I) nitrate, Poly(vinylpyrrolidone) M_n 55,000, sodium chloride (≥99.5%), L-ascorbic acid (≥99.0%), poly(ethylene glycol) methyl ether M_n 5,000, hydrazine solution 35 wt% in water, Nafion® 117 solution (~5% in a mixture of lower aliphatic alcohols and water), methanol (HPLC grade), potassium hydrogen carbonate (≥99.95%), anhydrous dimethyl sulfoxide (≥99.9%) and carbon monoxide, carbon dioxide, methane, ethane, ethylene and acetylene were purchased from Air Liquide. Sodium hydroxide (≥98.0%), Cu (II) nitrate (≥99.0%), ethanol (100%) and acetone (≥99.8%) were purchased from Sigma Aldrich. Nitric acid (69%) was purchased from VWR International Pty Ltd. Deuterium oxide (99.9%) was purchased from Sigma Aldrich.

Methods

All aqueous solutions were prepared using Milli-Q water.

Ag cores synthesis

Ag cores were synthesized according to a literature procedure. [1] Briefly, 175 mg poly(vinyl pyrrolidone) M_n 55,000 and 175 mg silver nitrate were dissolved in 40 mL water. To this solution, 0.4 mL 5.0 M sodium chloride was added under magnetic stirring. Further stirring for 15 min in the dark led to the formation of a colloidal suspension of AgCl nanoparticles. A solution containing 2.80 g ascorbic acid and 800 mg sodium hydroxide in 360 mL water was prepared. To this solution, the freshly prepared AgCl colloids were added under magnetic stirring with further stirring for 2 h in the dark. Using a centrifuge at 6000 rpm (4226 rcf) for 7 min, the reaction mixture was washed twice with water and concentrated to 100 mL and stored in the dark at 4 °C.

Au seeds synthesis

Au seeds were synthesized according to a literature procedure. [2] Briefly, 1 mL of 1% aqueous $HAuCl_4 \cdot 3H_2O$ was added to 100 mL of H_2O with vigorous stirring, followed one min later by addition of 1 mL of 1% aqueous sodium tricitrate. After an additional minute, 1 mL of 0.075% $NaBH_4$ in 1% sodium tricitrate was added. The solution was stirred for 5 min and then stored at 4 °C until needed.

Pd cores synthesis

Pd cores were synthesized according to a literature procedure. [3] Briefly, a 1000 mL solution of 2.0 mM H_2PdCl_4 was prepared by dissolving $PdCl_2$ (355 mg, 2.00 mmol) in HCl (1000 mL, 4.0 mM) by stirring and heating (~80 ºC) until the solution turned clear orange-yellow.

H_2O_2 (40.0 mL, 30%) was added to room temperature stirring solution of H_2PdCl_4 (1000 mL, 2.0 mM) and sodium tricitrate solution (100 mL, 1% w/w). 20 mL of the previously prepared Au seed solution was added to this solution. When the colour changed from yellow to grey the solution was washed twice with PVP M_n 55,000 solution (20 $g \cdot L^{-1}$) and once with water and then all ten batches were concentrated to 250 mL.

Porous Cu coating on Ag cores and Pd cores

Ag-core porous Cu-shell nanoparticles were synthesized using Ag cores with a procedure modified from the literature.[4] Briefly, poly(ethylene glycol) methyl ether M_n 5,000 solution (600 mL, 2 wt%), Ag nanoparticles (50.0 mL of the previously prepared suspension) and $Cu(NO_3)_2$ (10.0 mL, 0.1 M) were mixed under stirring. To this solution, hydrazine (300 µL, 35 wt%) was added and left stirring for 3 min. Using a centrifuge at 4000 rpm (1878 rcf) for 15 min, the reaction mixture was separated, and the product washed twice with water. Then using a centrifuge at 5000 rpm (2935 rcf) for 15 min, the reaction mixture was washed twice with ethanol and dried at 50 °C. Pd-core porous Cu-shell nanoparticles were synthesized with the same procedure but replacing the Ag nanoparticles with 80.0 mL of the previously prepared Pd cores suspension.

TEM

Transmission electron microscopy was performed with a JEM-2800 microscope (*JEOL*) equipped with Schottky-type emission source working at 200 kV and a Gatan OneView camera (4k*x*4k, 25FPS) to obtain images with a resolution of 0.09 nm. Energy dispersive spectroscopy elemental mapping was performed using double silicon drift detectors, with a solid angle of 0.98 steradians with a detection area of 100 mm^2. ~~TEM analysis for Figure S5 was performed on a CM200 (*Philips*) at 200 kV with a field emission gun.~~

Electrode preparation

H23 carbon paper (*Freudenberg*) was cut into pieces of 0.67 x 1.5 cm^2 area with a 0.4 x 3.5 cm^2 protrusion for contact and used as received. 4 drops of 27 µL each from a 7.5 mg·mL^{-1} catalyst suspension (1v% Nafion® in methanol) were drop-coated onto the carbon paper. The paper protrusion was disconnected during the drop-coating process by using two Teflon stripes mechanically pressed against each other. The paper was left to dry in air, resulting in an absolute loading of 0.8 mg of particles per electrode. *Ex-situ* control experiments were performed using circular glassy carbon electrodes with a diameter of 0.38 cm, which were drop-coated with 10 µL of the 7.5 mg·mL^{-1} catalyst suspension (in methanol) and left to dry for at least 2 h. The catalyst sample for the *ex-situ* TEM measurements was scraped off after electrocatalysis from the glassy carbon electrodes, which were previously drop-coated with the suspension of the pristine catalyst. A suspension of the aged catalyst was then prepared with ethanol and directly drop-coated onto a Au TEM grid for further TEM investigation.

Electrochemical setup

The H-type cell for the CO_2RR experiments with AgCu and PdCu nanozymes was custom-built. A Fumasep® FAA-3-PK-130 (*Fumatech*) anion exchange membrane was used to separate the two compartments. The gas flowrate was set to 5 mL·min^{-1} using a mass flow controller, which controlled the flow before the inlet into cathodic compartment. The cathodic and anodic compartments were filled with 0.1 M $KHCO_3$, pre-treated with Chelex® 100 resin. The electrolyte was pre-bubbled vigorously with CO_2 for 30 min before used for the cathodic compartment. 5.54 mL of electrolyte were filled into the cathodic compartment and a blank aliquot of 540 µL was taken before the reaction was started. Liquid aliquots of 540 µL were taken every 15 min and GC injections were automatically taken from the cathodic exhaust every 7.5 min. The working electrode was carbon paper and the reference electrode was a custom-built Ag|AgCl|3M KCl electrode. For every experiment, a new working electrode and fresh electrolyte were employed. Platinum mesh was used as the counter electrode. Chronoamperometry was run for 1 h at a fixed potential using an Autolab potentiostat controlled with the Nova software.

The *ex-situ* control experiments were performed using the circular glassy carbon electrodes, which were previously modified with catalyst. The electrodes were immersed in a beaker containing 40 mL 0.1 M $KHCO_3$, which was pre-treated with Chelex® 100 resin and saturated with CO_2 before use. Throughout the measurement, the electrolyte was continuously bubbled with CO_2. The CO control experiments were performed in 0.1 M $KHCO_3$, which was bubbled with gas containing 10% CO in He and ≥99.5% CO to obtain concentrations of 0.1 mM and 1 mM CO respectively. The used reference electrode was a commercial Ag|AgCl|3M KCl reference electrode (Metrohm). Platinum mesh was used as the counter electrode, which was separated from the main electrolyte by a frit. Chronoamperometry was run for 1 h at a fixed potential using an Autolab potentiostat controlled with the Nova software.

Potentials in all experiments were converted from vs. Ag|AgCl|3M KCl to vs. RHE using the following formula:

$$E_{RHE} = E_{Ag|AgCl|3M\ KCl} + 0.059 * pH + E^{\circ}_{Ag|AgCl|3M\ KCl},$$

where pH = 6.8 and $E^{\circ}_{Ag|AgCl|3M\ KCl}$ = 0.210 vs. SHE.

Liquid products were analysed using ^{1}H-NMR. 540 µL aliquots of electrolyte from the cathode compartment were taken before during and after electrocatalysis. Each aliquot was mixed with 60 µL of DMSO in D_2O stock solution. The DMSO in D_2O stock solution was prepared by mixing 5.0 µL DMSO with 10 mL D_2O. NMR aliquots were investigated on Bruker Avance III HD 400 MHz NMR with 64 scans and 16 s recycle delay, using DMSO as the internal standard. Product quantification was performed via the internal DMSO standard to determine the concentration of CO_2 reduction products.

Gas products were analysed using gas chromatography. SRI 8610C multiple gas analyser #1 gas chromatograph (SRI Instruments) was calibrated using H_2, CO, CH_4, C_2H_4 and C_2H_6 [1 vol% each component in N_2, analytical standard). This gas mixture was later diluted with CO_2 with different ratios, thus creating a curve with different analyte concentrations. Automatic injection of 1.0 mL gas aliquots was performed from the cathode gas exhaust every 7.5 min (Column HaySepD 3 metres, oven temperature 90 °C, run 6 min).

ELC-TEM (electrochemistry coupled liquid cell transmission electron microcopy)

The ELC-TEM measurement was performed using the liquid glassy carbon WE E-chip system with a 500 nm spacer and a Poseidon Select holder from *Protochips* (Figure S1 A-C). After the WE was mounted onto the holder, the holder was introduced to ultrahigh vacuum inside a vacuum turbopump (*Pfeiffer Vacuum*) to test for stability and potential leakage. During testing as well as the electrochemical measurement, electrolyte was flowing at 60 µL·h^{-1} through the active region using a glass syringe (*Hamilton*) and a syringe pump (*Harvard Apparatus*).

The procedure for the chip preparation was performed in accordance with a method described in literature.[5] For ELC-TEM measurements, the AgCu nanoparticles were deposited on the TEM chip by utilising a recently reported capillary-based approach. Nanocapillaries were prepared with a P-2000 laser-based micropipette puller (*Sutter*) using quartz capillaries of 1.2 and 0.9 mm outer and inner diameter, respectively. The pulled capillaries were filled with the catalyst suspension in ethanol using a MicroFil MF34G-5 needle (*World Precision Instruments*). A Pt-wire was inserted into the capillary and the ink-filled capillary was mounted on a specifically designed capillary holder. The WE on the ELC-TEM chip was connected via its Pt contact pad using a Cu tape and the chip was positioned on a piezo cube (*PI*) controlled by an E-663 analogue amplifier (*PI*). The piezo cube is fixed on a positioning system consisting of three stepper motors (*Owis*) controlled with a LStep PCIe controller (*Lang*). The stepper motors are used to pre-position the capillary at around 10 µm above the WE of the Si_3N_4 chip controlled optically with the aid of a video microscope camera.

The automatic approach is started with an approach speed of 100 nm·s^{-1}, while applying a voltage difference of 100 mV between the Pt-wire inside the capillary and the WE of the chip and monitoring the current with an ELC-03XS current amplifier (*npi*). Initially only noise is measured as the electric circuit is not closed, however, immediately upon contact of the drop hanging from the opening of the capillary with the surface, a distinct increase in the measured current signal is observed, which is used to stop the approach in an automatic feedback loop. The stop criterion was usually set to the detection of a current higher than 20 pA. The capillary is then retracted manually and moved to another position above the chip for the next approach to increase the catalyst loading. The setup is built on an RS 2000 vibration damping table (*Newport*) with S-2000 stabilisers (*Newport*) in a Faraday cage with thermal isolation panels. The piezo cube, stepper motors and current amplifier are controlled via a PCIe-7852R FPGA card (*National Instruments*) with a LabVIEW software adapted from the WEC-SPM software program obtained from the Unwin group (University of Warwick).

The WE of the ELC-TEM was held at -1.0 V vs. Pt-wire for a duration of 30 s before a potential step to -2.0 V vs. Pt was applied (Figure S1 d). Cathodic currents were recorded as a combination of a charging current and faradaic currents (CO_2RR as well as HER). A decay in applied potential was observed, which occurred due to a potential overload, since the CE could not readily maintain the electroneutrality of the nanoscopic system. The current decays similarly, which can be attributed to the decreasing driving force for faradaic reactions as well as dry areas on the working electrode due to gas evolution. The current approaches 0 µA for the first time after 258 s and ~~subsequently~~ again after 408 s, indicating that the whole working electrode ~~is~~ was either dry or not connected to

the CE via electrolyte any longer. Between 258 s and 408 s, however, cathodic currents ~~are~~ were ~~being~~ detected again, which ~~indicated~~ indicates that the WE was ~~re~~-wetted again, before it ~~eventually remained~~ became dry at ~~after~~ 408 s and remained that way . The region that was investigated in the video does not change anymore after 170 s indicating that the window was dried out in this part and hence no further decomposition of the catalyst was observed any longer. The electron dose during recording of the movie is 12.7 $e^{-}\cdot Å^{-2}\cdot s^{-1}$. The submitted movies M1 and M2 are played back in real-time at original magnification.

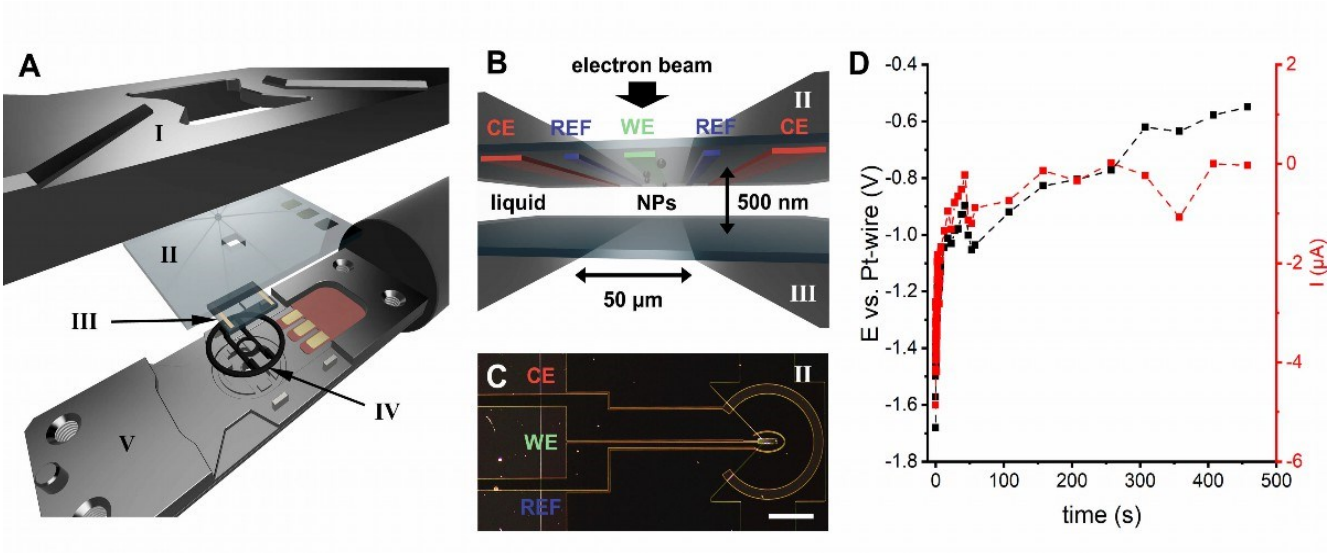

Figure S1. Schematic drawing of ELC-TEM cell, with components from top to bottom (a): lid (I), electrochemistry chip with electrodes (II, top part of liquid cell), chip with 500 nm spacer (III, bottom part of liquid cell), gasket (IV), TEM holder with contacts (V). Schematic side view (b) of liquid cell (II and III) consisting of counter electrode (red, CE), reference electrode (blue, REF), working electrode (green, WE), catalyst nanoparticles (black, NPs). Electron beam direction and liquid phase are indicated as well as spacer thickness (500 nm) and window width (50 µm). Top view of electrochemistry chip (II) with electrodes under a light microscope (c). Scale bar equals 500 µm. Electrodes are indicated at contact points. Chronoamperogram recorded during ELC-TEM measurement (d). Current in µA (red) is plotted versus time in seconds. Potential (black) is additionally plotted versus time. Potentials are given versus Pt-wire, which represents the real potential in the cell as well as versus RHE following the assumptions and the formula provided in the explanatory text below.

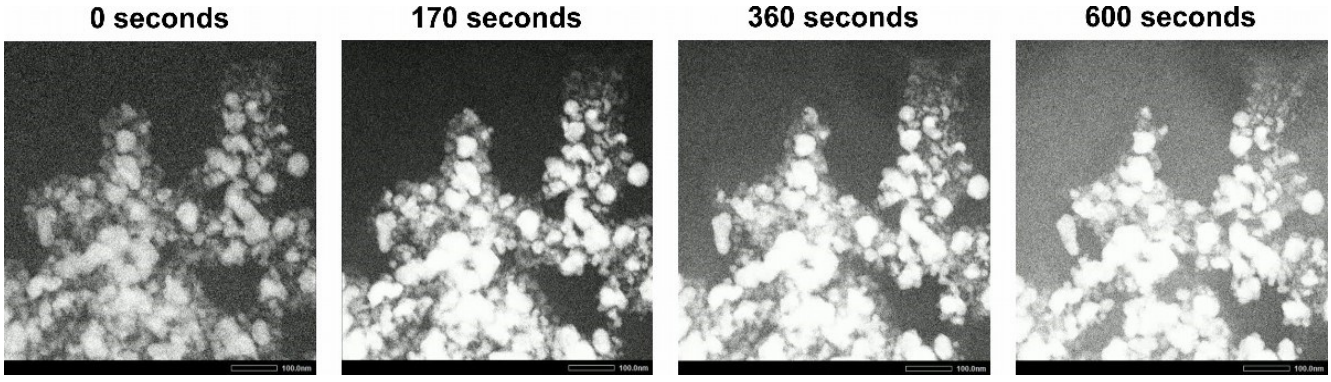

Figure S2. The impact of the electron beam on the Ag-core/porous Cu-shell nanoparticles. Some catalyst degradation was observed under the influence of the electron beam in the ELC-TEM cell at OCP in 0.1 M $KHCO_3$. However, such changes in the Cu phase (lower contrast) were observed only after 360 s which is beyond the timeframe of the experiment discussed in the main manuscript (170 s).

It is important to consider that several aspects are inherent to ELC-TEM that affect the interpretation of the results. These include a complicated potential control due to the use of a Pt pseudo-reference electrode in an electrolyte nanovolume, where small changes of the chemical environment can lead to substantial changes in the reference potential. The applied potential during the main video is referenced against a Pt wire. Referencing versus RHE was previously performed with a Pt-wire immersed in the same solution outside the TEM and includes

a shift of +272 mV *vs.* Ag/|AgCl/|3 M KCl in this electrolyte, and the additional shift of Ag/|AgCl/|3 M KCl of +611 mV *vs.* RHE resulting in a combined shift of +883 mV Pt *vs.* RHE. The effect of chemical changes in the ELC-TEM cell and the reductive power of the electron beam on the real WE potential are not taken into consideration. The isolated effect of the electron beam on the catalytic system is observable in CO_2-saturated 0.1 M $KHCO_3$, where no potential was applied and no changes of the catalyst material were observed over the timescale of the experiments reported in the main paper (Figure S2). The electron dose during recording of the control movie is 31.4 $e^{-}\cdot Å^{-2}\cdot s^{-1}$.

Importantly, it was shown that in the timeframe of the video discussed in the main manuscript (170 s) no observable changes occurred. After 360 s first changes in terms of Cu degradation occur, which then further increase until 600 s. These changes suggest that the reductive power of the electron beam alone induces CO_2RR at open circuit potential, which eventually leads to catalyst degradation. Therefore, the effect of applied potential and electron beam on the catalyst cannot be clearly differentiated, and a precise control of potential is not achievable under these circumstances. The lack of changes within the first 170 s, however, indicates that the changes observed in Figure S2 require potential and cannot be the result of the beam alone. We hypothesise that the reason for the lack of changes during the first 360s lies in the fact that a prolonged period of time is required to build up a sufficiently high local CO concentration within the pores to induce the structural evolution under the influence of the electron beam alone.

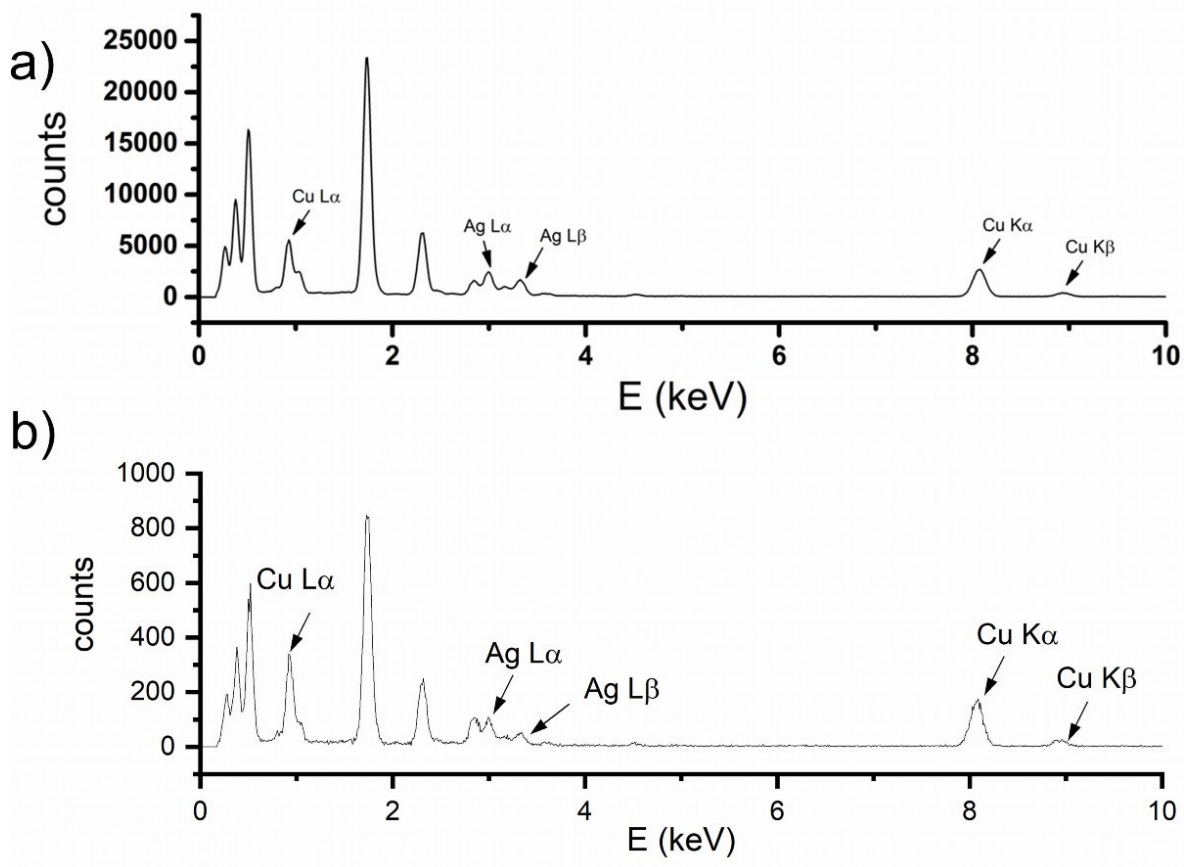

Figure S3. EDS spectra of the whole image in the ELC-TEM cell as in the final image in Figure 2a (a) and within the red rectangle of the same image (b) confirm the presence of Ag and Cu.

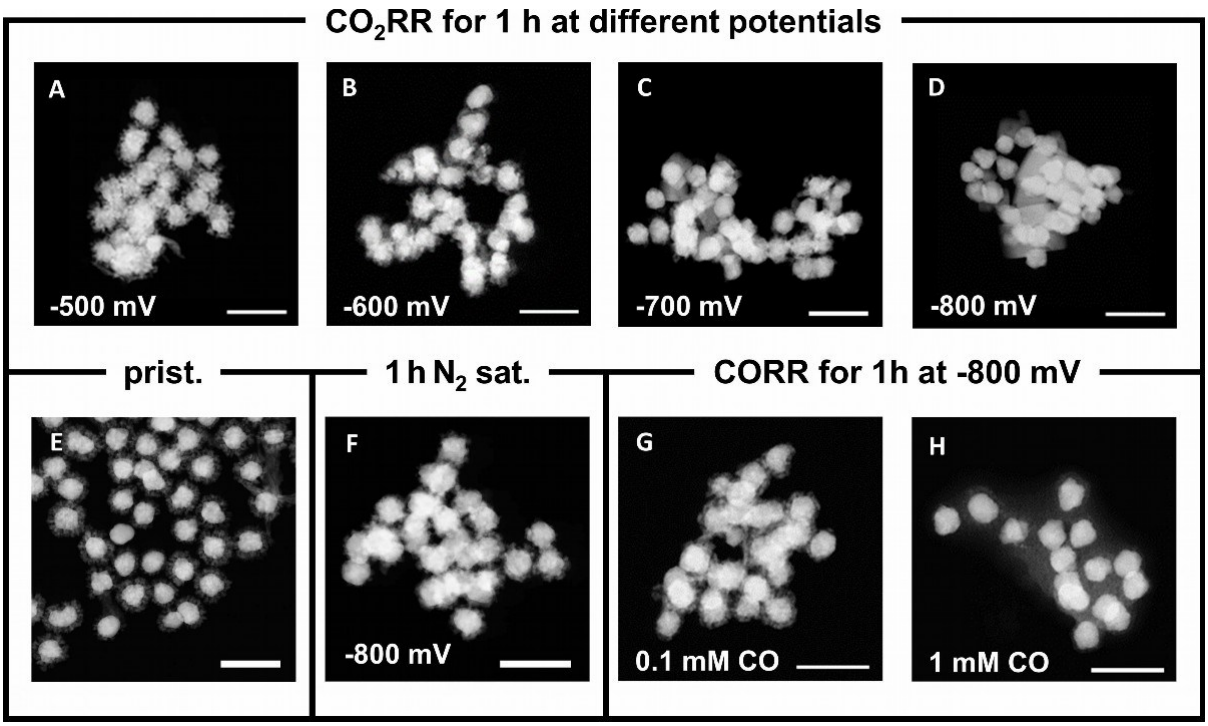

Figure S4. Dark field scanning TEM images of the energy-dispersive X-ray spectroscopy elemental maps provided in Figure 3 of the main manuscript. Scale bars equal 250 nm.

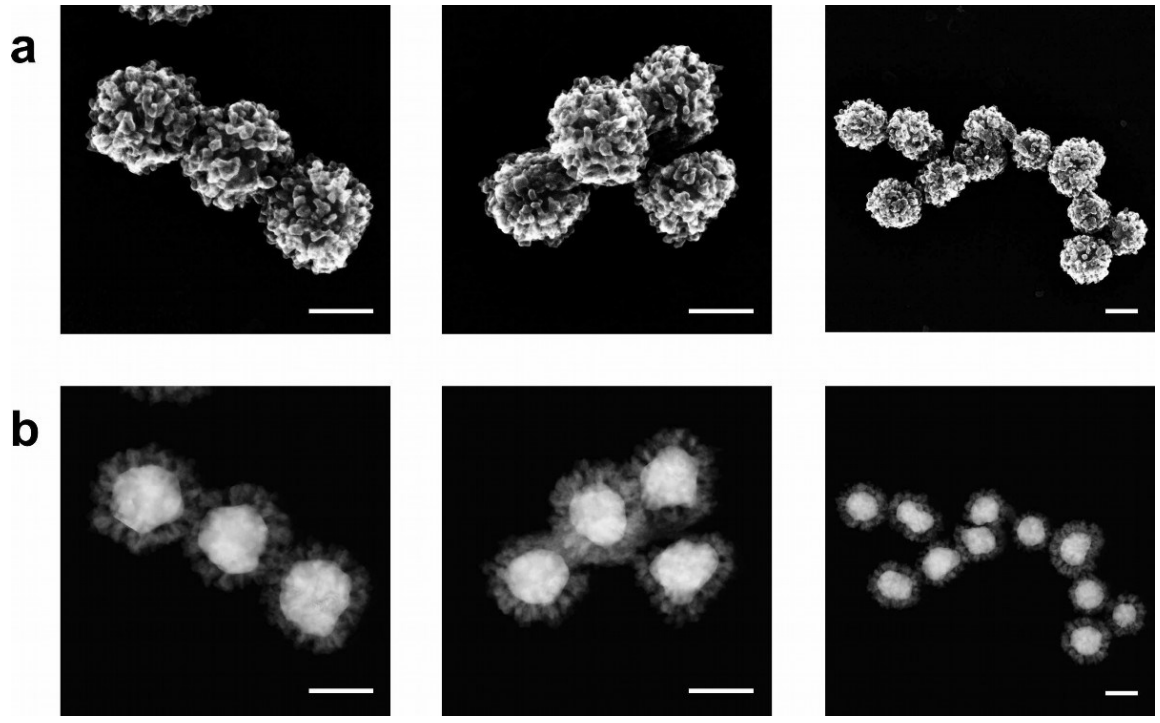

Figure S5. SEM (a) and STEM (b) images of the as-synthesised AgCu nanozyme particles. Particulates, which make up the shell, have ~10-15 nm diameter. Scale bars equal 100 nm.

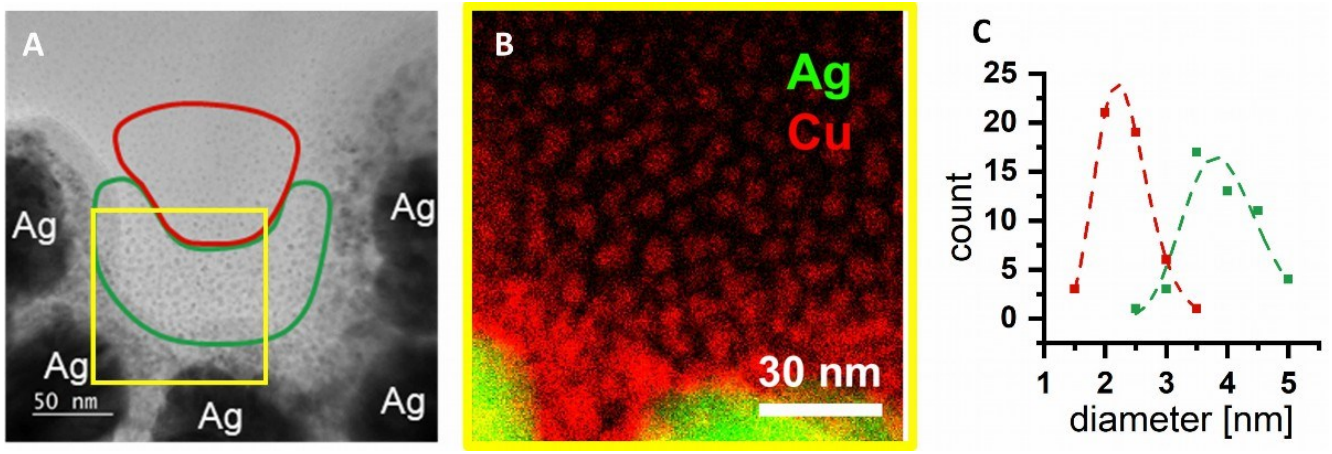

Figure S6. Cu nanoparticles observed after CO_2RR for 1 h at -600 mV vs. RHE (a). EDX elemental map (b) of the region indicated by the yellow box in (a). The Ag is depicted in green and Cu in red. Size distribution of the nanoparticles in the colour-coded regions using 2.5 nm bins and fit of the frequency count with the log-normal distribution based on 50 nanoparticles for each area (c).

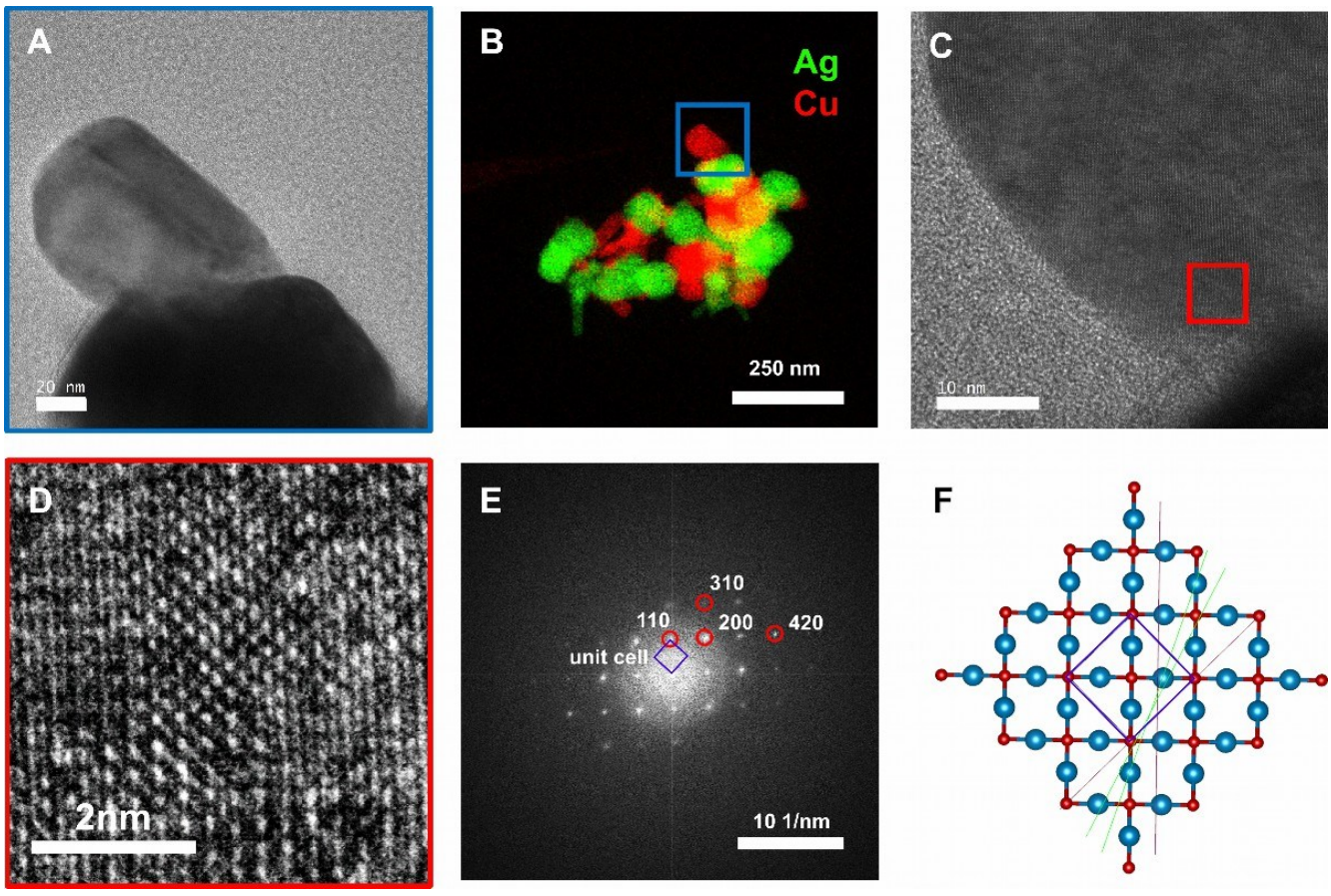

Figure S7. Single crystal formed after 1 h at -800 mV vs. RHE under CO_2RR conditions (a). EDX elemental map of the particle array including the particle from (a) as indicated by the blue box (b). The Ag is depicted in green and Cu in red. Highly crystalline region from the particle in (a) at higher magnification (c). HR-TEM image of red box in (c) showing lattice structure (d). Fourier transform of (d) with indicated lattice planes and cubic unit cell (e). The Fourier transform can be indexed and matched with Cu_2O viewed down the [001] orientation (f). The model was created using VESTA software 3.4.7 and data from ref.[6].

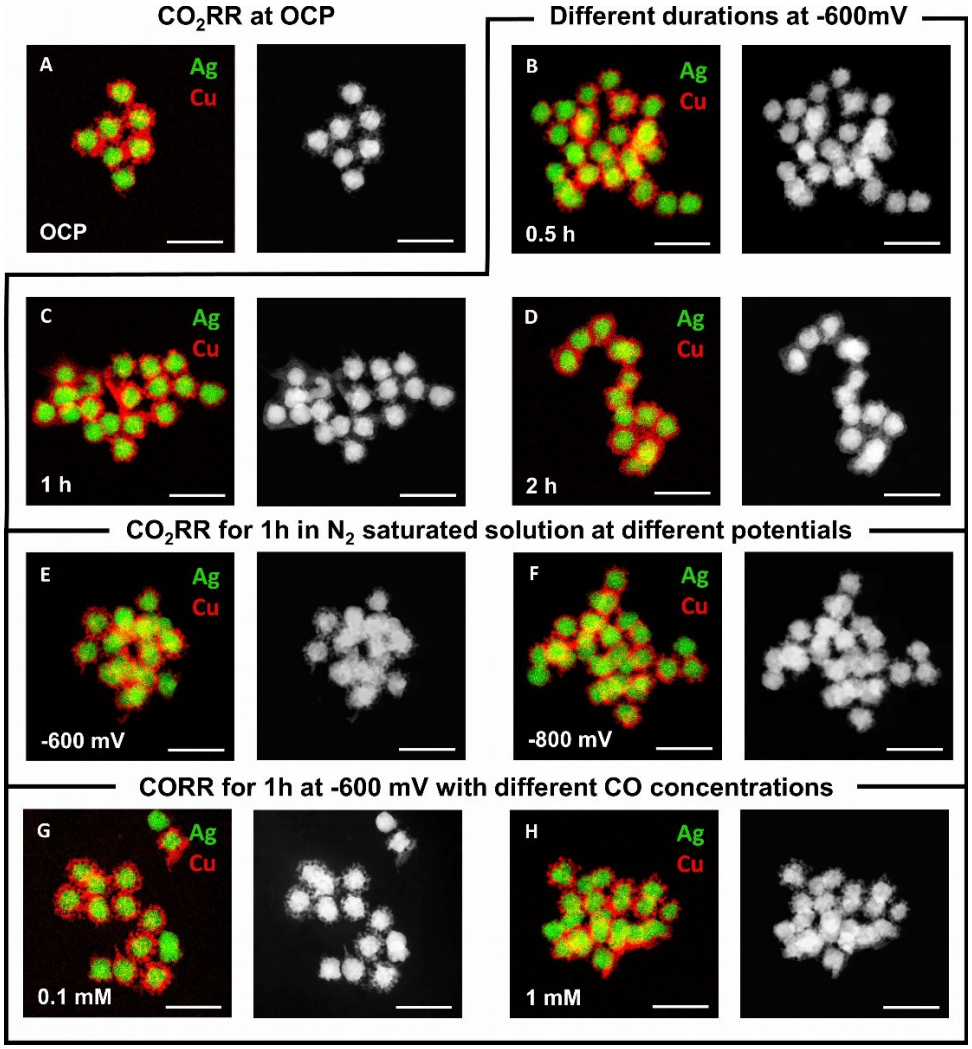

Figure S8. Investigation of the influencing factors on the structural evolution of AgCu catalysts in 0.1 M $KHCO_3$. Energy-dispersive X-spectroscopy elemental maps with the associated dark field scanning TEM images are presented. Catalyst material after 1 h at OCP in CO_2-saturated solution (a), after 0.5 h (b), 1 h (c) and 2 h (d) at -600 mV vs. RHE in CO_2-saturated solution, after 1 h in N_2-saturated solution at -600 mV vs. RHE (e) and -800 mV vs. RHE (f), after 1 h under CORR conditions at -600 mV vs. RHE in 0.1 M $KHCO_3$ containing 0.1 mM CO (g) and 1 mM CO (h). Scale bars equal 250 nm.

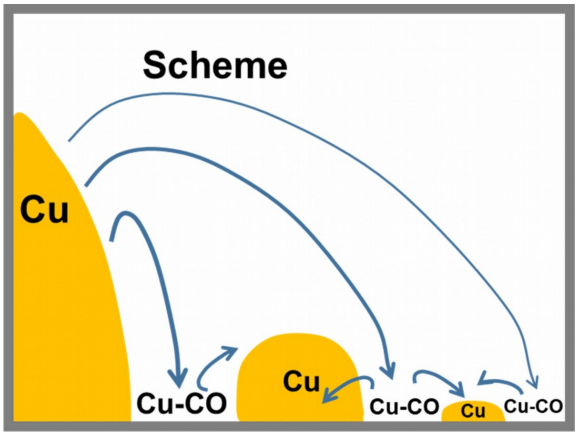

Figure S9. Proposed mechanisms of how copper nanoparticles are formed from the degradation of the copper in the AgCu core-shell nanoparticles: (i) primarily formed CO binds to Cu sites, (ii) weakens its binding strength to adjacent Cu atoms, (iii) removes Cu atoms from the under-coordinated sites of the particulates in the shell, which spread unidirectionally around the particulate of origin, and (iv) eventually aggregate to nanoparticles or single crystals. Scheme depicts the suggested Cu degradation mechanism, which explains the distance-dependent size distribution shown in Figure S6.

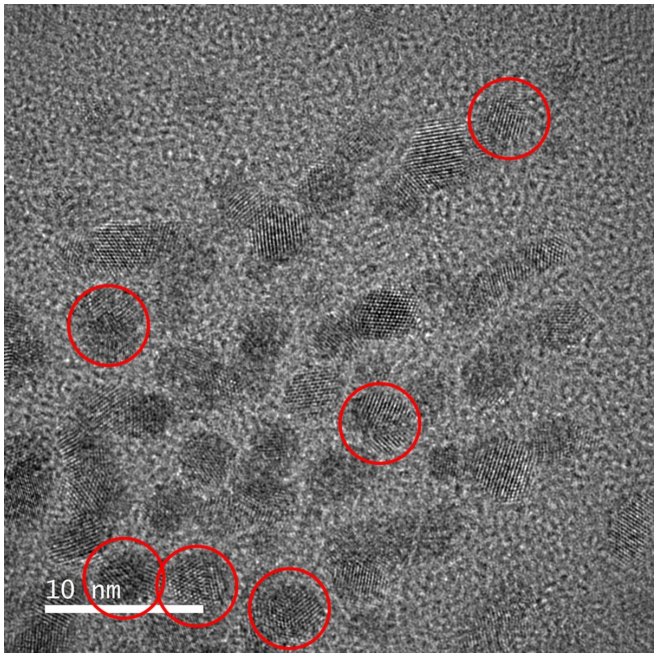

Figure S10. HR-TEM images of polycrystalline nanoparticles marked in red circles and single crystalline nanoparticles at a magnification of 20Mx.

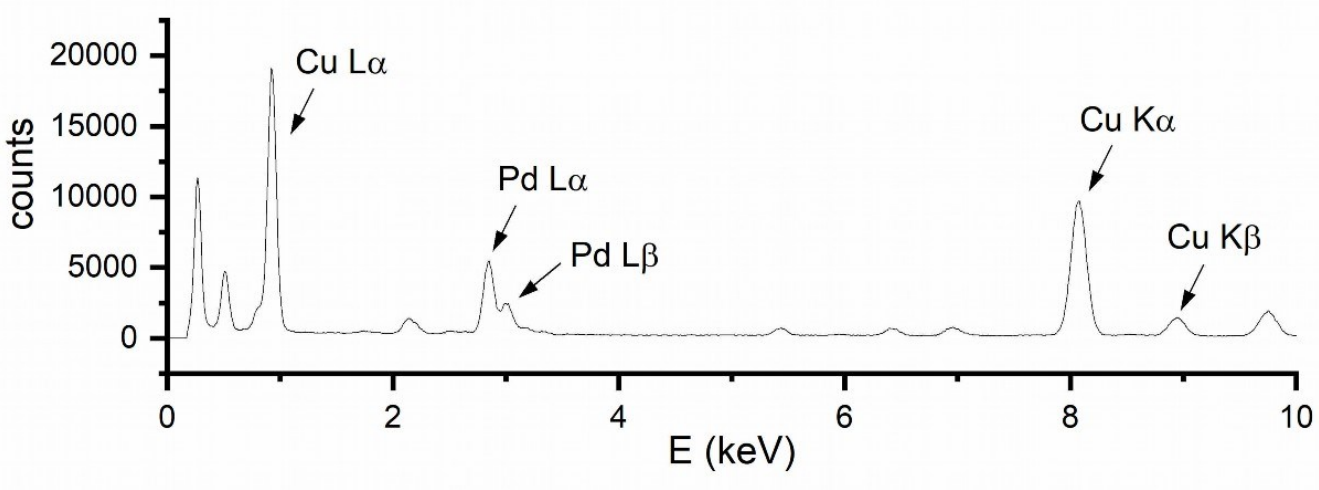

Figure S11. EDX spectrum of the pristine PdCu nanoparticles presented in Figure 4a.

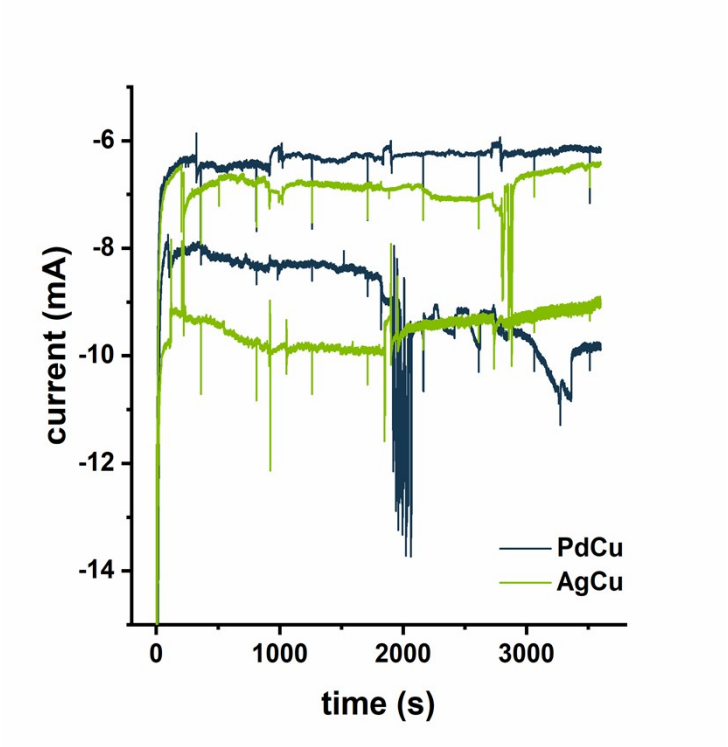

Figure S12. Chronoamperograms recorded during CO_2RR in 0.1 M $KHCO_3$ at -800 mV vs. RHE for 3600 s with AgCu (green) and PdCu (blue) solid core-porous shell nanoparticles. Current is plotted in mA versus time in s. Current irregularities were observed during taking of aliquots and during GC injections.

References

[1] B. Chen, X. Jiao, D. Chen, *Cryst. Growth Des.* **2010**, *10*, 3378.

[2] K. C. Grabar, K. J. Allison, B. E. Baker, R. M. Bright, K. R. Brown, R. G. Freeman, A. P. Fox, C. D. Keating, M. D. Musick, M. J. Natan, *Langmuir* **1996**, *12*, 2353.

[3] H. Chen, G. Wei, A. Ispas, S. G. Hickey, A. Eychmüller, *J. Phys. Chem. C* **2010**, *114*, 21976.

[4] L. Zhang, H. Jing, G. Boisvert, J. Z. He, H. Wang, *ACS Nano* **2012**, *6*, 3514.

[5] T. Tarnev, S. Cychy, C. Andronescu, M. Muhler, W. Schuhmann, Y.-T. Chen, *Angew. Chem. Int. Ed.* **2020**.

[6] M. C. Neuburger, *Z. Physik* **1931**, *67*, 845.